Selenophosphate Phase Diagrams Developed in Conjunction with the Synthesis of the New Compounds $K_2La(P_2Se_6)_{1/2}(PSe_4)$, $K_3La(PSe_4)_2$, $K_4La_{0.67}(PSe_4)_2$, $K_{9-x}La_{1+x/3}(PSe_4)_4$ ($x = 0.5$), and $KEuPSe_4$

Carl R. Evenson IV and Peter K. Dorhout*,†

Department of Chemistry, Colorado State University, Fort Collins, Colorado 80523

Received June 2, 2000

Five new rare-earth metal polyselenophosphates have been synthesized by the reactive flux method and characterized by single-crystal X-ray diffraction: $K_2La(P_2Se_6)_{1/2}(PSe_4)$ (**I**), $K_3La(PSe_4)_2$ (**II**), $K_4La_{0.67}(PSe_4)_2$ (**III**), $K_{9-x}La_{1+x/3}(PSe_4)_4$ ($x = 0.5$) (**IV**), and $KEuPSe_4$ (**V**). Compound **I** crystallizes in the monoclinic space group $P2_1/n$ with $a = 9.4269(1)$ Å, $b = 7.2054(1)$ Å, $c = 21.0276(5)$ Å, $\beta = 97.484(1)°$, and $Z = 4$. Compound **II** crystallizes in the monoclinic space group $P2_1/c$ with $a = 9.5782(2)$ Å, $b = 17.6623(4)$ Å, $c = 9.9869(3)$ Å, $\beta = 90.120(1)°$, and $Z = 4$. Compound **III** crystallizes in the orthorhombic space group *Ibam* with $a = 19.0962(2)$ Å, $b = 9.1408(1)$ Å, $c = 10.2588(2)$ Å, and $Z = 4$. Compound **IV** crystallizes in the orthorhombic space group *Ccca* with $a = 18.2133(1)$ Å, $b = 38.0914(4)$ Å, $c = 10.2665(1)$ Å, and $Z = 8$. Compound **V** crystallizes in the orthorhombic space group *Pnma* with $a = 17.5156(11)$ Å, $b = 7.0126(5)$ Å, $c = 6.9015(4)$ Å, and $Z = 4$. Optical band gap measurements show that compound **V** has an optical band gap of 1.88 eV. Solid-state Raman spectroscopy of compounds **II**−**V** shows the four normal vibrations expected for the $(PSe_4)^{3-}$ unit. The observation of compounds **I**−**V** in several reactions has allowed the creation of a quasi-quaternary phase diagram for potassium rare-earth-metal polyselenophosphates. This phase diagram can qualitatively be separated into three regions on the basis of the oxidation state of phosphorus in the crystalline products observed and takes the next step in designing solid-state compounds.

Introduction

In the past several years there has been considerable interest in the synthesis of new rare-earth metal (RE) selenide compounds using the reactive flux method.[1−8] While the literature of transition-metal compounds synthesized by this method is quite extensive,[9−25] lanthanide and actinide compounds have received much less attention.[1,24,26−34] Of those, several new ternary and quaternary rare-earth metal selenophosphate structures have been reported, including $K(RE)P_2Se_6$ (RE = Y, La, Ce, Pr, Gd),[1] $K_3CeP_2S_8$,[29] $A_2(RE)P_2Se_7$ (A = Rb, Cs; RE =

* To whom correspondence should be addressed. E-mail: pkd@LAMAR.colostate.edu.

† P.K.D. is a Camille Dreyfus Teacher Scholar and an A. P. Sloan Fellow.

(1) Chen, J. H.; Dorhout, P. K.; Ostenson, J. E. *Inorg. Chem.* **1996**, *35*, 5627−5633.
(2) Chen, J. H.; Dorhout, P. K. *J. Solid State Chem.* **1995**, *117*, 318−322.
(3) Cody, J. A.; Mansuetto, M. F.; Chien, S.; Ibers, J. A. *Mater. Sci. Forum* **1994**, *152*−*153*, 35−42.
(4) Evain, M.; Brec, R.; Whangbo, M.-H. *J. Solid State Chem.* **1987**, *71*, 244−262.
(5) Kanatzidis, M. G. *Chem. Mater.* **1990**, *2*, 353−363.
(6) Kanatzidis, M. G.; Huang, S.-P. *Coord. Chem. Rev.* **1994**, *130*, 509−621.
(7) Kanatzidis, M. G.; Sutorik, A. C. *Prog. Inorg. Chem.* **1995**, *43*, 151−265.
(8) Kanatzidis, M. G. *Curr. Opin. Solid State Mater. Sci.* **1997**, *2*, 139−149.
(9) Chondroudis, K.; Kanatzidis, M. G. *Inorg. Chem.* **1995**, *34*, 5401−5402.
(10) Chondroudis, K.; McCarthy, T. J.; Kanatzidis, M. G. *Inorg. Chem.* **1996**, *35*, 840−844.
(11) Chondroudis, K.; Kanatzidis, M. G. *Chem. Commun.* **1996**, 1371−1372.
(12) Chondroudis, K.; Kanatzidis, M. G. *Angew. Chem., Int. Ed. Engl.* **1997**, *36*, 1324−1326.
(13) Chondroudis, K.; Kanatzidis, M. G.; Sayettat, J.; Jobic, S.; Brec, R. *Inorg. Chem.* **1997**, *36*, 5859−5868.
(14) Chondroudis, K.; Hanko, J. A.; Kanatzidis, M. G. *Inorg. Chem.* **1997**, *36*, 2623−2632.
(15) Chondroudis, K.; Kanatzidis, M. G. *Inorg. Chem.* **1998**, *37*, 2098−2099.
(16) Chondroudis, K.; Kanatzidis, M. G. *J. Solid State Chem.* **1998**, *136*, 79−86.
(17) Chondroudis, K.; Kanatzidis, M. G. *Inorg. Chem.* **1998**, *37*, 2848−2849.
(18) Dorhout, P. K.; Malo, T. M. *Z. Anorg. Allg. Chem.* **1996**, *622*, 385−391.
(19) Hanko, J. A.; Sayettat, J.; Jobic, S.; Brec, R.; Kanatzidis, M. G. *Chem. Mater.* **1998**, *10*, 3040−3049.
(20) Kanatzidis, M. G.; Park, Y. *Chem. Mater.* **1990**, *2*, 99−101.
(21) Marking, G. A.; Hanko, J. A.; Kanatzidis, M. G. *Chem. Mater.* **1998**, *10*, 1191−1199.
(22) McCarthy, T. J.; Kanatzidis, M. G. *Inorg. Chem.* **1995**, *34*, 1257−1267.
(23) Payen, C.; McMillan, P.; Colombet, P. *Eur. J. Solid State Inorg. Chem.* **1990**, *27*, 881−896.
(24) Sutorik, A. C.; Albritton-Thomas, J.; Kannewurf, C. R.; Kanatzidis, M. G. *J. Am. Chem. Soc.* **1994**, *116*, 7706−7713.
(25) Tremel, W.; Kleinke, H.; Derstroff, V.; Reisner, C. *J. Alloys Compd.* **1995**, *219*, 73−82.
(26) Briggs Piccoli, P. M.; Abney, K. D.; Schoonover, J. R.; Dorhout, P. K. *Inorg. Chem.*, in press.
(27) Chen, J. H.; Dorhout, P. K. *Inorg. Chem.* **1995**, *34*, 5705−5706.
(28) Chen, J. H.; Dorhout, P. K. *J. Alloys Compd.* **1997**, *249*, 199−205.
(29) Gauthier, G.; Jobic, S.; Brec, R.; Rouxel, J. *Inorg. Chem.* **1998**, *37*, 2332−2333.
(30) Chondroudis, K.; Kanatzidis, M. G. *Inorg. Chem. Commun.* **1998**, *1*, 55−57.
(31) Chondroudis, K.; Kanatzidis, M. G. *Inorg. Chem.* **1998**, *37*, 3792−3797.
(32) Chondroudis, K.; Kanatzidis, M. G. *J. Am. Chem. Soc.* **1997**, *119*, 2574−2575.
(33) Patschke, R.; Brazis, P.; Kannewurf, C. R.; Kanatzidis, M. G. *Inorg. Chem.* **1998**, *37*, 6562−6563.

10.1021/ic000595z CCC: $20.00 © 2001 American Chemical Society
Published on Web 05/10/2001

Table 1. Crystallographic Data for $K_2La(P_2Se_6)_{1/2}(PSe_4)$, $K_3La(PSe_4)_2$, $K_4La_{0.67}(PSe_4)_2$, $K_{9-x}La_{1+x/3}(PSe_4)_4$ ($x = 0.5$), and $KEuPSe_4$

	$K_2LaP_2Se_7$ (**I**)	$K_3La(PSe_4)_2$ (**II**)	$K_4La_{0.67}(PSe_4)_2$ (**III**)	$K_{9-x}La_{1+x/3}(PSe_4)_4$ (**IV**)	$KEuPSe_4$ (**V**)
fw	831.77	949.83	943.09	1881.42	537.87
a, Å	9.42690(10)	9.5782(2)	19.0962(2)	18.2133(1)	17.5156(11)
b, Å	7.20540(10)	17.6623(4)	9.14080(10)	38.0914(4)	7.0126(5)
c, Å	21.0276(5)	9.9869(3)	10.2588(2)	10.2665(1)	6.9015(4)
α, deg	90.0	90.0	90.0	90.0	90.0
β, deg	97.4840(10)	90.1200(10)	90.0	90.0	90.0
γ, deg	90.0	90.0	90.0	90.0	90.0
V, Å^3	1416.12(4)	1689.51(7)	1790.72(4)	7122.59(11)	847.71(9)
Z	4	4	4	8	4
λ(Mo Kα), Å	0.71073	0.71073	0.71073	0.71073	0.71073
space group	$P2_1/n$ (no. 14)	$P2_1/c$ (no. 14)	*Ibam* (no. 72)	*Ccca* (no. 68)	*Pnma* (no. 62)
temp, K	298(2)	170(2)	159(2)	158(2)	170(2)
ρ_{calcd}, Mg/m^3	3.901	3.734	3.498	3.209	4.214
μ, mm^{-1}	21.775	20.657	18.957	18.919	25.150
R1,[a] %	4.29	4.76	3.53	5.43	2.37
wR2,[a] %	8.90	10.36	7.55	11.44	5.23

[a] $R1 = \sum(|F_o| - |F_c|)/\sum|F_o|$. $wR2 = [\sum[w(F_o^2 - F_c^2)^2]/\sum[w(F_o^2)^2]]^{1/2}$.

Ce, Gd),[31] $K_4Eu(PSe_4)_2$,[10] and $KCeSe_4$.[35] Many of these new compounds have been made using an alkali-metal polychalcophosphate reactive flux. This particular reactive flux seems to be well suited for the moderate to high temperature synthesis of RE compounds. Different polychalcophosphate units are believed to be stabilized within the flux and coordinate well to RE cations. Some units such as $(P_2Q_6)^{4-}$ and $(PQ_4)^{3-}$ (Q = S, Se) seem to be very stable and are observed in many different structures. while other units such as $(PQ_5)^{3-}$, $(P_2Q_7)^{2-}$, and $(P_2Q_7)^{4-}$ are much rarer. The reason one unit forms over another under certain reaction conditions has not been fully understood.

The concept of Lewis basicity has been used to help explain why different crystalline products are observed for different reactant mixtures and reaction conditions.[7] For example, more alkali-metal rich reactant mixtures for a given amount of chalcogen yield a more Lewis basic flux. Fluxes with different Lewis basicities appear to stabilize different anionic units in the liquid flux, where they can coordinate to alkali-metal and RE cations. While this Lewis basicity argument partially explains the reason certain types of products are observed, it does not explain all phases observed. A more detailed analysis would involve a careful investigation of the quaternary phase space in the K−RE−P−Se system.

In the process of trying to find new rare-earth-metal polyselenophosphate compounds, we have begun to develop ternary phase diagrams for the crystalline products observed for a series of similar reactions. Contained in the K−La−P−Se and K−Eu−P−Se phase diagrams reported here are the new compounds **I**−**V**, for which some structure types are known, as well as some products previously reported in the literature and observed in our reactions.

Experimental Section

Synthesis. Crystals of all compounds observed were obtained using the same basic procedure. The following reactants were used as received and stored in an inert atmosphere glovebox: La (99.999%, Ames Laboratory), Eu (99.95%, Ames Laboratory), P (Mallinckrodt Red), Se (99.999%, Johnson-Mathey), and SrSe (99.5%, Cerac). K_2Se and K_2Se_4 were previously made in liquid ammonia from the stoichiometric combination of the elements.[36,37] Reactants were loaded into fused silica ampules inside the glovebox. Each ampule was flame sealed under vacuum and placed in a temperature-controlled tube furnace. The furnace was ramped to 725 °C, where it remained for 150 h. The furnace was then allowed to cool back to room temperature at 4 °C/h. Crystalline products were separated from excess flux with dimethylformamide (DMF).

$K_2La(P_2Se_6)_{1/2}(PSe_4)$ (I) was prepared by reacting 38.4 mg (0.486 mmol) of Se, 69.7 mg (0.181 mmol) of K_2Se_4, 8.22 mg (0.265 mmol) of P, and 12.3 mg (0.089 mmol) of La. The reaction was carried out as described above, yielding dark yellow crystals.

$K_3La(PSe_4)_2$ (II) was prepared by reacting 38.9 mg (0.493 mmol) of Se, 139.0 mg (0.353 mmol) of K_2Se_4, 13.1 mg (0.423 mmol) of P, and 19.6 mg (0.141 mmol) of La. The reaction was carried out as described above, producing yellow crystals.

$K_4La_{0.67}(PSe_4)_2$ (III) was prepared by reacting 19.4 mg (0.246 mmol) of Se, 96.8 mg (0.246 mmol) of K_2Se_4, 7.6 mg (0.246 mmol) of P, 34.1 mg (0.246 mmol) of La, and 20.5 mg (0.123 mmol) of SrSe. Reactants were combined and reacted as described above. The finished reaction revealed yellow crystals. Sr was not included in the crystalline product.

$K_{9-x}La_{1+x/3}(PSe_4)_4$ ($x = 0.5$) (IV) was prepared from the reaction of 82.3 mg (1.04 mmol) of Se, 48.2 mg (0.307 mmol) of K_2Se, 7.6 mg (0.245 mmol) of P, and 17.0 mg (0.122 mmol) of La. The reaction product contained dark yellow crystals.

$KEuPSe_4$ (V) was obtained by reacting 39.8 mg (0.504 mmol) of Se, 29.4 mg (0.0746 mmol) of K_2Se_4, 4.6 mg (0.149 mmol) of P, and 23.5 mg (0.155 mmol) of Eu. Following the reaction procedure described above yielded dark red crystals.

Physical Measurements. Single-Crystal X-ray Diffraction. Intensity data sets for crystals I−V were collected using a Bruker SMART CCD diffractometer. Each intensity data set was integrated using SAINT,[38] a SADABS correction was applied,[39] and the structure was solved by direct methods using SHELXTL.[40] Crystallographic data for compounds **I**−**V** are reported in Table 1.

Raman Spectroscopy. The solid-state Raman spectra of compounds **II**−**V** were taken with a Nicolet Magna-IR spectrometer with a FT-Raman module attachment using a Nd:YAG excitation laser (1064 nm).

UV−Vis Spectroscopy. A diffuse reflectance measurement for $KEuPSe_4$ was taken with a Hitachi U-3501 spectrophotometer using a 60 mm diameter integrating sphere accessory and $BaSO_4$ sample and reference plates. UV−vis diffuse reflectance data were converted to optical band gap data using the Kubelka−Munk function.[41,42]

(34) Sutorik, A. C.; Kanatzidis, M. G. *Chem. Mater.* **1997**, *9*, 387−398.
(35) Sutorik, A. C.; Kanatzidis, M. G. *Angew. Chem., Int. Ed. Engl.* **1992**, *31*, 1594−1596.
(36) Liao, J.-H.; Kanatzidis, M. G. *Inorg. Chem.* **1992**, *31*, 431−439.
(37) Schewe-Miller, I. *Metallreiche hauptgruppenmetall-Chalkogenverbindungen: Synthese, Strukturen und Eigenschaften*; Max-Planck-Institut fur Festkorperforschung: Stuttgart, Germany, 1990.
(38) *Data processing software for the SMART system*; Bruker Analytical X-ray Instruments Inc.: Madison, WI, 1995.
(39) Sheldrick, G. M. *SADABS*; University of Gottingen: Gottingen, Germany, 1997.
(40) *SHELXTL 5.03*; Bruker Analytical X-ray Systems Inc.: Madison, WI, 1994.
(41) McCarthy, T. J.; Tanzer, T. A.; Kanatzidis, M. G. *J. Am. Chem. Soc.* **1995**, *117*, 1294−1301.

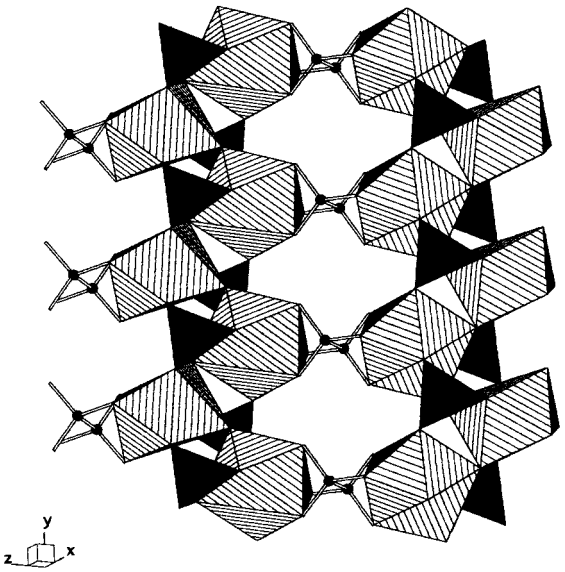

Figure 1. $K_2La(P_2Se_6)_{1/2}(PSe_4)$: striped La−Se polyhedra, black $(PSe_4)^{3-}$ tetrahedra, black phosphorus atoms in $(P_2Se_6)^{4-}$. Potassium atoms left out for clarity.

Energy Dispersive Spectroscopy. Semiquantitative microprobe analysis of compounds **III** and **IV** was performed on a Philips 505 scanning electron microscope equipped with a Kevex Analyst 8000 microanalyzer.

Results and Discussion

Structures. A single crystal of $K_2La(P_2Se_6)_{1/2}(PSe_4)$ or $K_2LaP_2Se_7$ **(I)** was selected, 8862 (3365 independent) reflections were collected, and an absorption correction was applied ($R_{int} = 0.0513$). The structure was solved in $P2_1/n$ by direct methods to electron density residuals of 1.285 and −1.503 e Å^{-3}, and all atoms were refined anisotropically with SHELXTL using full-matrix least-squares refinement on F^2 for 110 variables.[40] $K_2LaP_2Se_7$ is a layered structure containing quasi-infinite layers of $^2_\infty[La(P_2Se_6)_{1/2}(PSe_4)]^{2-}$ in the (101) plane of the unit cell. These layers are separated by 9-coordinate potassium atoms with an average K−Se distance of 3.592(9) Å. Figure 1 shows that these layers comprise chains of La−Se polyhedra coordinated by $(PSe_4)^{3-}$ tetrahedra. Along each chain, each $(PSe_4)^{3-}$ tetrahedron is coordinated to three different lanthanum atoms. Two La−Se polyhedra share a common vertex and share an edge with one $(PSe_4)^{3-}$ tetrahedron. The chain propagates via another corner-shared La−Se polyhedron and a shared $(PSe_4)^{3-}$ tetrahedron. These chains are linked together by $(P_2Se_6)^{4-}$ units to form a layer. Eight selenium atoms with an average La−Se distance of 3.141(3) Å coordinate each lanthanum atom in a distorted square antiprism. Atomic coordinates and selected bond distances for $K_2La(P_2Se_6)_{1/2}(PSe_4)$ can be found in Tables 2 and 3, respectively. Several other compounds with similar structures have been reported, including $Cs_2TbP_2Se_7$ and $K_2YP_2Se_7$,[43] $K_2CeP_2S_7$,[29] and $Rb_2CeP_2Se_7$ and $Cs_2GdP_2Se_7$.[31]

A single crystal of $K_3La(PSe_4)_2$ **(II)** was selected, 10987 (4059 independent) reflections were collected, and an absorption correction was applied ($R_{int} = 0.0478$). The structure was solved in $P2_1/c$ by direct methods to electron density residuals of 2.658 and −1.607 e Å^{-3}, and all atoms were refined anisotropically with SHELXTL using full-matrix least-squares refinement on F^2 for 127 variables.[40] The structure of $K_3La(PSe_4)_2$ consists of anionic $^1_\infty[La(PSe_4)_2]^{3-}$ chains that run along the *x* axis of the unit cell. These chains are separated by potassium cations. Along the length of the chain, 8-coordinate lanthanum atoms are separated by two $(PSe_4)^{3-}$ tetrahedra in which one Se atom on each $(PSe_4)^{3-}$ tetrahedron bridges two neighboring La atoms. Figure 2A shows two different long La···La distances that arise from the alternating orientation of bridging Se atoms. Where the bridging Se atoms and two La atoms (for example, La(1) and La(1D)) form a plane parallel to the *ab* plane, the La···La distance is 5.292 Å. Where the bridging Se atoms and La atoms (for example, La(1B) and La(1C)) form a plane parallel to the

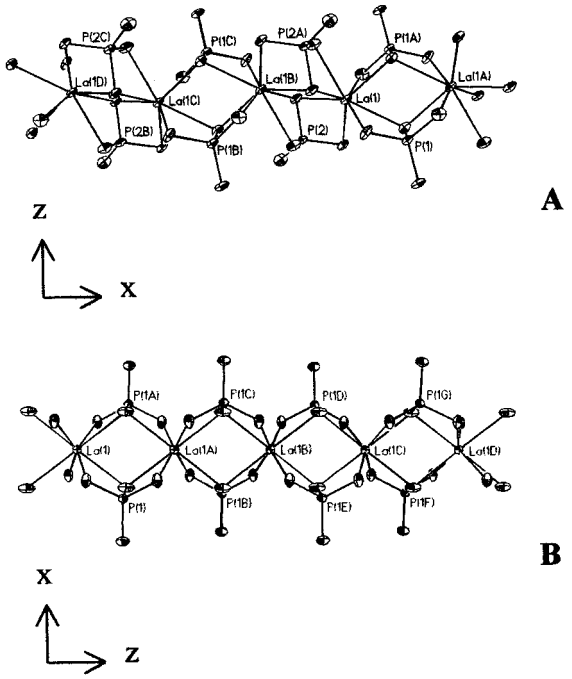

Figure 2. ORTEP plots of the (A) $[La(PSe_4)_2]^{3-}$ chain and (B) $[La_{0.67}(PSe_4)_2]^{4-}$ chain. Thermal ellipsoids plotted at the 70% probability level. Unlabeled selenium atoms. Potassium atoms left out for clarity.

Table 2. Fractional Atomic Coordinates and Equivalent Isotropic Displacement Parameters (Å$^2 \times 10^3$)[a] for $K_2La(P_2Se_6)_{1/2}(PSe_4)$

	x	y	z	*U*(eq)
La(1)	0.8072(1)	0.4726(1)	0.1499(1)	19(1)
Se(1)	0.7175(1)	0.4614(1)	−0.0040(1)	26(1)
Se(2)	0.5838(1)	0.7758(1)	0.1045(1)	27(1)
Se(3)	0.8091(1)	0.0780(1)	0.2192(1)	23(1)
Se(4)	1.0527(1)	0.4794(1)	0.2592(1)	34(1)
Se(5)	1.0565(1)	0.2591(1)	0.0991(1)	26(1)
Se(6)	1.0224(1)	0.7511(1)	0.0967(1)	25(1)
Se(7)	0.5281(1)	0.2543(1)	0.1068(1)	27(1)
P(1)	0.5933(2)	1.0164(3)	0.1685(1)	18(1)
P(2)	0.9184(2)	0.4903(3)	−0.0432(1)	20(1)
K(1)	1.2576(2)	0.0075(3)	0.0091(1)	40(1)
K(2)	1.3425(3)	0.5411(4)	0.1865(1)	54(1)

[a] *U*(eq) is defined as one-third of the trace of the orthogonalized U_{ij} tensor.

Table 3. Selected Bond Distances (Å) for $K_2La(P_2Se_6)_{1/2}(PSe_4)$

La(1)−Se(4)	3.0421(10)	La(1)−Se(7)	3.0979(10)
La(1)−Se(2)	3.0980(9)	La(1)−Se(5)	3.1127(9)
La(1)−Se(6)	3.1609(9)	La(1)−Se(3)	3.1829(9)
La(1)−Se(3)	3.1937(9)	La(1)−Se(1)	3.2380(9)
P(1)−Se(7)	2.189(2)	P(1)−Se(4)	2.195(2)
P(1)−Se(3)	2.217(2)	P(2)−Se(5)	2.184(2)
P(2)−Se(6)	2.184(2)	P(2)−Se(1)	2.171(2)
P(1)−Se(2)	2.189(2)	P(2)−P(2)	2.226(4)

(42) Wilkinson, F.; Kelly, G. In *Diffuse Reflectance Flash Photolysis*; Scaiano, J. C., Ed.; CRC Press: Boca Raton, FL, 1989; Vol. 1, pp 293−314.
(43) Van Calcar, P.; Evenson, C. R.; Dorhout, P. K. Unpublished results.

Table 4. Fractional Atomic Coordinates and Equivalent Isotropic Displacement Parameters ($Å^2 \times 10^3$)[a] for $K_3La(PSe_4)_2$

	x	y	z	*U*(eq)
La(1)	0.2266(1)	0.0138(1)	0.9704(1)	17(1)
Se(1)	−0.0365(1)	0.1268(1)	0.9681(1)	22(1)
Se(2)	0.0567(1)	0.0186(1)	1.2558(1)	24(1)
Se(3)	0.5378(1)	0.0246(1)	0.8193(1)	19(1)
Se(4)	0.3088(1)	−0.1320(1)	0.8226(1)	25(1)
Se(5)	0.2172(1)	0.1166(1)	0.7183(1)	25(1)
Se(6)	−0.1278(1)	0.1815(1)	0.6308(1)	28(1)
Se(7)	0.5709(1)	−0.1259(1)	0.5680(1)	25(1)
Se(8)	0.3325(1)	0.1611(1)	1.0911(1)	24(1)
P(1)	0.5251(2)	−0.0991(1)	0.7750(2)	17(1)
P(2)	−0.0077(3)	0.1036(1)	0.7507(2)	17(1)
K(1)	0.1195(3)	0.2058(2)	1.3727(3)	43(1)
K(2)	0.3826(3)	−0.2855(2)	0.6259(3)	47(1)
K(3)	0.2699(2)	−0.0323(1)	0.5138(2)	31(1)

[a] *U*(eq) is defined as one-third of the trace of the orthogonalized U_{ij} tensor.

Table 5. Selected Bond Distances (Å) for $K_3La(PSe_4)_2$

La(1)−Se(8)	3.0403(11)	P(1)−Se(7)	2.167(2)
La(1)−Se(5)	3.1060(11)	P(2)−Se(1)	2.228(3)
La(1)−Se(3)	3.1533(11)	P(2)−Se(2)	2.209(3)
La(1)−Se(2)	3.2856(10)	P(1)−Se(3)	2.232(3)
La(1)−Se(4)	3.0712(11)	P(1)−Se(4)	2.204(2)
La(1)−Se(1)	3.1406(11)	P(2)−Se(5)	2.191(3)
La(1)−Se(1)	3.2152(11)	P(2)−Se(6)	2.155(3)
La(1)−Se(3)	3.3496(10)	P(1)−Se(8)	2.200(3)

bc plane, the La···La distance is 4.409 Å. Atomic coordinates and selected bond distances for $K_3La(PSe_4)_2$ can be found in Tables 4 and 5, respectively. Compounds with similar structures reported in the literature include $K_3CeP_2S_8$[29] and $Rb_3CeP_2Se_8$ and $Cs_3GdP_2Se_8$.[31]

A single crystal of $K_4La_{0.67}(PSe_4)_2$ or $K_6La(PSe_4)_3$ **(III)** was selected, 5519 (1150 independent) reflections were collected, and an absorption correction was applied ($R_{int} = 0.0413$). The structure was solved by direct methods in *Ibam* to electron density residuals of 1.367 and −1.477 e $Å^{-3}$, and all atoms were refined anisotropically with SHELXTL using full-matrix least-squares refinement on F^2 for 42 variables.[40] On the basis of its formula, one would expect $K_4La_{0.67}(PSe_4)_2$ to have a structure similar to that of $K_3La(PSe_4)_2$; indeed, they are related as they both contain chains of lanthanum atoms coordinated by $(PSe_4)^{3-}$ tetrahedra. In $K_4La_{0.67}(PSe_4)_2$, the $_{\infty}^{1}[La_{0.67}(PSe_4)_2]^{4-}$ chains propagate along the *z* axis. Unlike in the $K_3La(PSe_4)_2$ structure, the $(PSe_4)^{3-}$ tetrahedra in $_{\infty}^{1}[La_{0.67}(PSe_4)_2]^{4-}$ are orientated with their nonbridging Se vertexes in the same direction as seen in Figure 2B. The average La−Se bond distance is 3.256(2) Å compared to an average La−Se bond distance of 3.170(3) Å in $K_3La(PSe_4)_2$. Another significant difference is that the lanthanum position in $K_4La_{0.67}(PSe_4)_2$ is partially occupied to satisfy the charge-balancing requirements of the structure. On average, every third lanthanum atom is "missing", resulting in significantly shorter "chains" than the quasi-infinite chains found in $K_3La(PSe_4)_2$. Semiquantitative energy dispersive spectroscopy was performed on three different crystals, giving an average composition of $K_{3.86}La_{0.81}P_{2.24}Se_{7.77}$. Atomic coordinates and selected bond distances for $K_4La_{0.67}(PSe_4)_2$ can be found in Tables 6 and 7, respectively. $K_4La_{0.67}(PSe_4)_2$ is isotypic with $K_4Eu(PSe_4)_2$.[10]

A single crystal of $K_{9-x}La_{1+x/3}(PSe_4)_4$ ($x = 0.5$) **(IV)** was selected, 21677 (4392 independent) reflections were collected, and an absorption correction was applied ($R_{int} = 0.0855$) for an orthorhombic solution. The structure was solved by direct methods to electron density residuals of 1.774 and −1.935 e $Å^{-3}$, and all atoms were refined anisotropically with SHELXTL using full-matrix least-squares refinement on F^2 for 140 variables.[40] The initial monoclinic unit cell chosen by SMART [$a = 21.1980(1)$ Å, $b = 10.3100(1)$ Å, $c = 18.2874(1)$ Å, $\beta = 115.541(1)°$] was very similar to the unit cell of $Rb_9Ce(PSe_4)_4$[30] [$a = 21.446(5)$ Å, $b = 10.575(5)$ Å, $c = 18.784(4)$ Å, $\beta = 115.94(2)°$], and we therefore predicted a structure with the formula $K_9La(PSe_4)_4$ containing isolated $_{0}^{0}[La(PSe_4)_4]^{9-}$ anionic clusters. However, an acceptable structure solution could not be obtained in the expected *C*2/*c* space group. It was suggested that in this monoclinic space group the structure might exist as a merohedral twin; however, we were unable to model this solution. Significant election density was left on one of the potassium sites, leading to a structure with a lanthanum ratio higher than 1 and a formula that could not be charge balanced. We then looked to a system of higher symmetry based on a unit cell transformation to an orthorhombic cell, *Ccca*, with lattice parameters $a = 18.2133(1)$ Å, $b = 38.0914(4)$ Å, and $c = 10.2665(1)$ Å. In this cell a reasonable structure solution was found with the formula $K_{9-x}La_{1+x/3}(PSe_4)_4$ ($x = 0.5$). The structure of $K_{9-x}La_{1+x/3}(PSe_4)_4$ ($x = 0.5$) contains two different crystallographically distinct lanthanum atoms. The first lanthanum exists as isolated $_{0}^{0}[La(PSe_4)_4]^{9-}$ clusters like those observed for the $Rb_9Ce(PSe_4)_4$ structure. These clusters alternate with potassium atoms along the *z* axis of the unit cell as shown in Figure 3. The second lanthanum is found in chains of lanthanum atoms linked together by $(PSe_4)^{3-}$ tetrahedra along the *z* axis of the unit cell. The lanthanum position along these chains is 2/3 occupied, just as in the $K_4La_{0.67}(PSe_4)_2$ structure. The two different lanthanum positions alternate throughout the structure. $_{\infty}^{1}[La_{0.67}(PSe_4)_2]^{4-}$ chains alternate with $_{0}^{0}[La(PSe_4)_4]^{9-}$ clusters along the *x* axis and *y* axis. Both lanthanum atoms exist as dodecahedra with eight La−Se bonds. The average La−Se bond to each lanthanum shows the difference in environments. The average La−Se bond around each La(1) cluster is 3.125(3) Å, while the average La−Se bond length around each La(2) in a partially occupied chain is 3.256(5) Å. Semiquantitative energy dispersive spectroscopy was performed on three different crystals, giving an average composition of $K_{7.02}La_{1.06}P_{4.13}Se_{17.46}$. We have also synthesized the isostructural compounds $K_{9-x}Y_{1+x/3}(PSe_4)_4$ and $Rb_{9-x}La_{1+x/3}(PSe_4)_4$. The formation of $K_{9-x}La_{1+x/3}(PSe_4)_4$ ($x = 0.5$) instead of $K_9La(PSe_4)_4$ is discussed later in terms of dimensionality and the position of these quaternary structures within a ternary phase diagram. Atomic coordinates and selected bond distances for $K_{9-x}La_{1+x/3}(PSe_4)_4$ ($x = 0.5$) can be found in Tables 8 and 9, respectively.

Table 6. Fractional Atomic Coordinates and Equivalent Isotropic Displacement Parameters ($Å^2 \times 10^3$)[a] for $K_4La_{0.67}(PSe_4)_2$

	x	y	z	*U*(eq)
La(1)[b]	0.5000	0.0000	0.2500	14(1)
Se(1)	0.4218(1)	0.3012(1)	0.3271(1)	23(1)
Se(2)	0.3939(1)	0.0324(1)	0.0000	27(1)
Se(3)	0.2586(1)	0.2530(1)	0.5000	24(1)
P(1)	0.3710(1)	0.2054(2)	0.5000	14(1)
K(1)	0.4168(1)	0.3812(2)	0.0000	32(1)
K(2)	0.2572(1)	0.0000	0.2500	39(1)

[a] *U*(eq) is defined as one-third of the trace of the orthogonalized U_{ij} tensor. [b] The La(1) position is only 2/3 occupied.

Table 7. Selected Bond Distances (Å) for $K_4La_{0.67}(PSe_4)_2$

La(1)−Se(1) × 4	3.2305(6)	P(1)−Se(1)	2.2029(13)
La(1)−Se(2) × 4	3.2812(5)	P(1)−Se(1′)	2.2029(13)
P(1)−Se(2)	2.218(2)	P(1)−Se(3)	2.190(2)

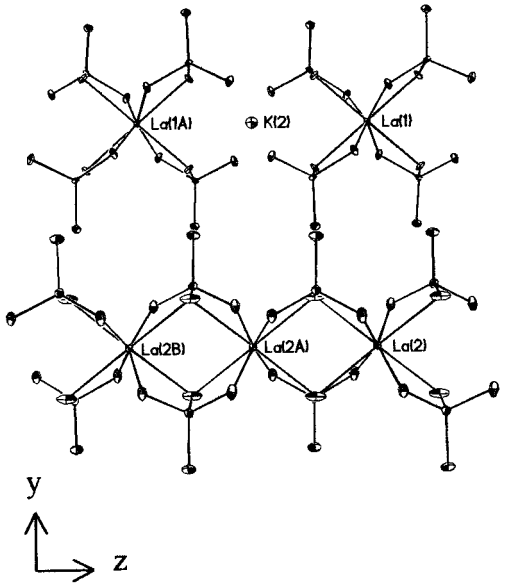

Figure 3. ORTEP plot of the different lanthanum coordination environments in $K_{9-x}La_{1+x/3}(PSe_4)_4$ ($x = 0.5$). Thermal ellipsoids plotted at the 50% probability level.

Table 8. Fractional Atomic Coordinates and Equivalent Isotropic Displacement Parameters ($Å^2 \times 10^3$)[a] for $K_{9-x}La_{1+x/3}(PSe_4)_4$ ($x = 0.5$)

	x	y	z	*U*(eq)
La(1)	0.0000	0.2500	0.7500	6(1)
La(2)[b]	−0.2500	0.0000	0.7535	9(1)
Se(1)	0.0155(1)	0.1965(1)	0.5229(1)	12(1)
Se(2)	0.1493(1)	0.2867(1)	0.6790(1)	14(1)
Se(3)	−0.1269(1)	0.1291(1)	0.5148(1)	17(1)
Se(4)	−0.1546(1)	0.2079(1)	0.3353(1)	17(1)
Se(5)	−0.4005(1)	0.0394(1)	0.3307(1)	21(1)
Se(6)	−0.4010(1)	0.0388(1)	0.6750(1)	24(1)
Se(7)	−0.3770(1)	0.1208(1)	0.5040(1)	23(1)
Se(8)	−0.2340(1)	0.0535(1)	0.5040(1)	32(1)
K(1)	0.1893(2)	0.2916(1)	1.0138(2)	23(1)
K(2)	0.0000	0.2500	0.2500	30(1)
K(3)	0.0000	0.1259(1)	0.7500	28(1)
K(4)	−0.0600(2)	0.0406(1)	0.5001(2)	30(1)
K(5)	−0.2533(1)	0.1216(1)	0.7609(2)	29(1)
K(6)	0.0000	0.1324(2)	0.2500	43(1)
P(1)	−0.1035(2)	0.1845(1)	0.5084(2)	7(1)
P(2)	−0.3531(2)	0.0636(1)	0.5039(2)	15(1)

[a] *U*(eq) is defined as one-third of the trace of the orthogonalized U_{ij} tensor. [b] The La(2) position is only 2/3 occupied.

Table 9. Selected Bond Distances (Å) for $K_{9-x}La_{1+x/3}(PSe_4)_4$ ($x = 0.5$)

La(1)−Se(1) × 4	3.1077(11)	P(1)−Se(2)	2.228(3)
La(1)−Se(2) × 4	3.1424(11)	P(1)−Se(3)	2.153(4)
La(2)−Se(5) × 2	3.2234(14)	P(1)−Se(4)	2.195(3)
La(2)−Se(6) × 2	3.2246(14)	P(2)−Se(5)	2.181(3)
La(2)−Se(8) × 2	3.285(2)	P(2)−Se(6)	2.176(3)
La(2)−Se(8′) × 2	3.293(2)	P(2)−Se(7)	2.220(5)
P(1)−Se(1)	2.221(4)	P(2)−Se(8)	2.204(5)

A single crystal of $KEuPSe_4$ (**V**) was selected, 5130 (1080 independent) reflections were collected, and an absorption correction was applied. Systematic absence analysis and a low R_{int} (0.0368) confirmed the correct space group choice of *Pnma*. The structure was solved by direct methods to electron density residuals of 0.829 and −1.193 e $Å^{-3}$, and all atoms were refined anisotropically with SHELXTL using full-matrix least-squares refinement on F^2 for 41 variables.[40] The structure for $KEuPSe_4$ was recently reported by Kanatzidis et al., which was solved as a twinned structure in the monoclinic space group $P2_1/m$ with cell parameters $a = 6.8469(6)$ Å, $b = 6.9521(6)$ Å, $c = 9.0436(8)$ Å, and $\beta = 107.677(2)°$.[44] Switching the reported *a* axis and *c* axis, transforming from a monoclinic cell to an orthorhombic cell, and finally doubling the new *a* axis gave cell parameters similar to ours of $a = 17.2338$ Å, $b = 6.9521$ Å, and $c = 6.8469$ Å; however, we note here that our reaction conditions were different from those reported by Kanatzidis et al. Their reaction conditions may have led to poor-quality, twinned crystals or a phase of slightly different structural organization. Our $KEuPSe_4$ is isotypic to $CsPbPSe_4$,[10] a layered material with lead atoms intricately linked by $(PSe_4)^{3-}$ tetrahedra.

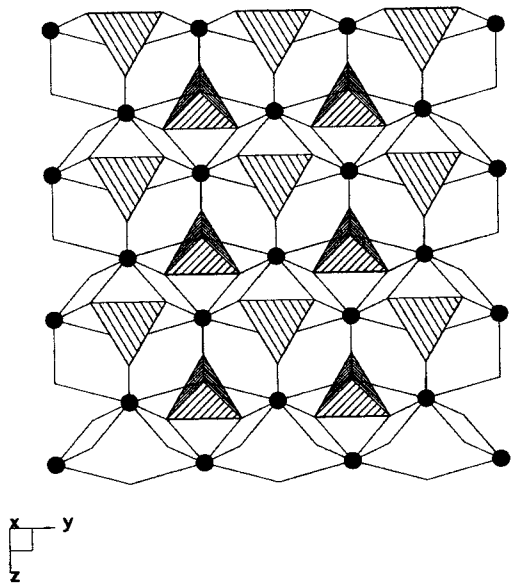

Figure 4. $(EuPSe_4)^-$ layer: black Eu circles, $(PSe_4)^{3-}$ tetrahedra.

In our $KEuPSe_4$, each $^2_\infty[EuPSe_4]^-$ layer is formed from a zigzag layer of europium atoms coordinated by alternating $(PSe_4)^{3-}$ units above and below the europium atoms. These layers are separated by potassium cations. Viewed down the *a* axis, Figure 4, each layer contains alternating $(PSe_4)^{3-}$ tetrahedra and 8-coordinate europium atoms as bicapped trigonal prisms. In this way, each $(PSe_4)^{3-}$ tetrahedron is coordinated to four different europium bicapped trigonal prisms in an edge-sharing manner. The 8-coordinate europium atom contains six shorter Eu−Se bonds (3.1324(8)−3.2259(5) Å) and two longer Eu−Se bonds (3.6374(3) Å). The long Eu−Se bonds are the capping Eu−Se bonds and result from a selenium atom bridging two alternating europium atoms. These two long bonds were not observed in the $CsPbPSe_4$ structure; however, an 8-coordinate divalent europium atom is more reasonable than a 6-coordinate divalent europium atom. Divalent europium atoms with this type of coordination have been observed before in Eu_2BiS_4[45] and $Eu_3Sb_4S_9$.[46] Atomic coordinates and selected bond distances for $KEuPSe_4$ can be found in Tables 10 and 11, respectively.

Phase Diagrams. La−P−K System. Figure 5 shows the quasi-quaternary Gibbs-type phase diagram for La−P−K. This ternary phase diagram is used to represent quaternary phase

(44) Aitken, J. A.; Chondroudis, K.; Young, V. G.; Kanatzidis, M. G. *Inorg. Chem.* **2000**, *39*, 1525−1533.
(45) Lemoine, P. P.; Carre, D.; Guittard, M. *Acta Crystallogr.* **1982**, *B38*, 727−729.
(46) Lemoine, P. P.; Carre, D.; Guittard, M. *Acta Crystallogr.* **1981**, *B37*, 1281−1284.

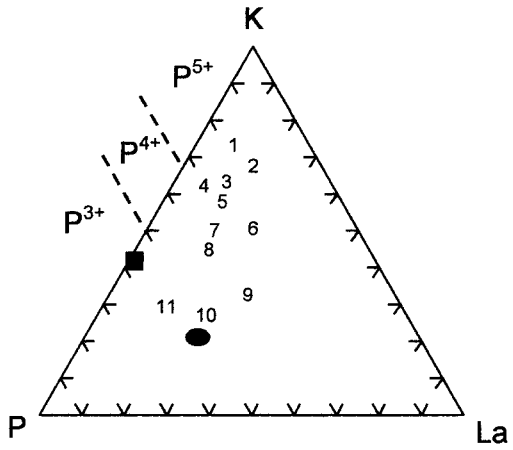

Figure 5. La−P−K ternary phase diagram. Numbers represent the ratio of La−P−K in a particular reaction mixture. Shapes indicate the ratio of elements in a product formula disregarding Se: circle = $KLaP_2Se_6$, square = $K_6P_8Se_{18}$.

Table 10. Fractional Atomic Coordinates and Equivalent Isotropic Displacement Parameters ($Å^2 \times 10^3$)[a] for $KEuPSe_4$

	x	y	z	*U*(eq)
Eu(1)	0.4754(1)	0.2500	0.2893(1)	15(1)
Se(1)	0.3274(1)	0.2500	0.0341(1)	17(1)
Se(2)	0.4727(1)	−0.2500	0.1492(1)	18(1)
Se(3)	0.3795(1)	−0.0028(1)	0.5947(1)	15(1)
P(1)	0.4035(1)	0.2500	−0.2212(2)	10(1)
K(1)	0.2135(1)	0.2500	0.4768(2)	25(1)

[a] *U*(eq) is defined as one-third of the trace of the orthogonalized U_{ij} tensor.

Table 11. Selected Bond Distances (Å) for $KEuPSe_4$

Eu(1)−Se(1)	3.1324(8)	Eu(1)−Se(2)	3.1598(8)
Eu(1)−Se(3)	3.1793(5)	Eu(1)−Se(3)	3.1793(5)
Eu(1)−Se(3)	3.2259(5)	Eu(1)−Se(3)	3.2259(5)
Eu(1)−Se(2)	3.6374(3)	Eu(1)−Se(2)	3.6374(3)
P(1)−Se(3)	2.2208(10)	P(1)−Se(3′)	2.2208(10)
P(1)−Se(2)	2.225(2)	P(1)−Se(1)	2.209(2)

Table 12. Reactant Ratios Represented in Figure 5

phase diagram point (#)	K/(K + P + La)	P/(K + P + La)	La/(K + P + La)	reaction product(s)
1	0.7272	0.1818	0.0909	$K_{9-x}La_{1+x/3}(PSe_4)_4$
2	0.667	0.1667	0.1667	
3	0.625	0.25	0.125	
4	0.6153	0.308	0.0769	$K_{9-x}La_{1+x/3}(PSe_4)_4$ and $K_3La(PSe_4)_2$
5	0.5714	0.2857	0.1429	
6	0.5	0.25	0.25	$K_4La_{0.67}(PSe_4)_2$
7	0.5	0.3333	0.1667	$K_3La(PSe_4)_2$ and $K_2La(P_2Se_6)_{1/2}(PSe_4)$
8	0.4545	0.3636	0.1818	$K_2La(P_2Se_6)_{1/2}(PSe_4)$
9	0.3333	0.3333	0.3333	
10	0.25	0.5	0.25	$KLaP_2Se_6$
11	0.2857	0.5714	0.1429	$KLaP_2Se_6$ and $K_6P_8Se_{18}$

space wherein the reactions were all performed with a constant selenium content and under a relative thermodynamic equilibrium isotherm of 725 °C. In these phase diagrams, numbers represent reactions wherein various ratios of K/(K + P + La), P/(K + P + La), and La/(K + P + La) were used. Table 12 lists the ratio of respective components for each phase diagram point. In this way, the quasi-quaternary La−P−K phase diagrams can be thought of as an isometric selenium slice through the quaternary La−P−K−Se phase diagram.

In Figure 5, six different crystalline products are represented: $K_{9-x}La_{1+x/3}(PSe_4)_4$ ($x = 0.5$) (**IV**), $K_4La_{0.67}(PSe_4)_2$ (**III**), $K_3La(PSe_4)_2$ (**II**), and $K_2La(P_2Se_6)_{1/2}(PSe_4)$ (**I**); two additional phases, $KLaP_2Se_6$[27] and $K_6P_8Se_{18}$,[47] were observed as crystalline reaction products, but have been reported elsewhere. At high potassium molar ratios and low phosphorus and lanthanum molar ratios (points 1−3), compound **IV** was the only crystalline product observed. Increasing the molar ratio of phosphorus and decreasing the molar ratio of potassium in the reactant mixture changes which crystalline products are observed in the reactions. Compounds **IV** and **II** were observed at points 4 and 5, and compound **III** was found at point 6. Up to this position in the phase diagram, only structures with $(PSe_4)^{3-}$ units are observed. However, as the phosphorus molar ratio was increased and the potassium molar ratio was decreased, we observed compound **I** at points 7−9, which contain both $(PSe_4)^{3-}$ and $(P_2Se_6)^{4-}$ units. Continuing in a similar manner, there is a region of the phase diagram containing only $(P_2Se_6)^{4-}$ units as seen in $KLaP_2Se_6$ (point 12), and finally, at high phosphorus concentrations we observed $K_6P_8Se_{18}$ as a reaction product in addition to $KLaP_2Se_6$ at point 13. The significance of the different $(P_xSe_y)^{n-}$ units observed may be attributed to the relative oxidation state of phosphorus and, therefore, the relative oxidizing power of the flux. In $(PSe_4)^{3-}$ phosphorus is P^V, $(P_2Se_6)^{4-}$ contains P^{IV}, and $K_6P_8Se_{18}$ contains P^{III}. This trend is logical since the amount of material that needs to be oxidized (P, La) is increased for a given Se^0/Se^{2-} composition. Both phosphorus and lanthanum need to be oxidized, and when the $P/(Se^0/Se^{2-})$ or $La/(Se^0/Se^{2-})$ ratios are too high, there is insufficient oxidizing power to oxidize phosphorus to higher oxidation states. On the basis of the oxidation state of phosphorus, the phase diagram can be divided qualitatively into three regions. A line separating P^V and P^{IV} can be drawn approximately between points 6 and 7 at a 35% phosphorus molar ratio, and a line separating P^{IV} and P^{III} can be drawn approximately at a 50% phosphorus molar ratio.

There is a strong correlation between reactant ratios and the position of products on this phase diagram. For example, if a tie-line exists between $KLaP_2Se_6$ (black circle) and $K_6P_8Se_{18}$ (black square) under these reaction conditions, then a reaction with K−P−La ratios corresponding to point 13 should yield both crystalline products. This was observed experimentally. This same type of relationship is found for the other crystalline compounds. We can therefore conclude that, under these isometric, isothermal reaction conditions, we have identified all the stable phases in this region of the phase diagram.

Eu−P−K System. The Eu−P−K phase diagram, Figure 6, is very similar to the lanthanum version, but with fewer stable phases found under our isometric and isothermal reaction conditions. Four crystalline products have been observed so far and are listed in Table 13: $KEuPSe_4$, reported here, $K_4Eu(PSe_4)_2$,[10] $K_6P_8Se_{18}$,[47] and $Eu_2P_2Se_6$, which is isostructural with $Eu_2P_2S_6$.[48]

In this phase diagram, P^V is represented by the $K_4Eu(PSe_4)_2$ (points 1−3) and $KEuPSe_4$ (point 4) structures. This P^V region of the phase diagram seems to extend farther into the phosphorus-rich region than in the lanthanum diagram. This can be rationalized by the fact that europium is only oxidized to Eu^{2+} instead of Eu^{3+}; given the relative redox couples of lanthanum vs europium, there is more oxidizing agent available for the oxidation of phosphorus. Structures with P^{IV} were not observed

(47) Chondroudis, K.; Kanatzidis, M. G. *Inorg. Chem.* **1998**, *37*, 2582−2584.
(48) Brockner, W.; Becker, R. *Z. Naturforsch.* **1987**, *42a*, 511−512.

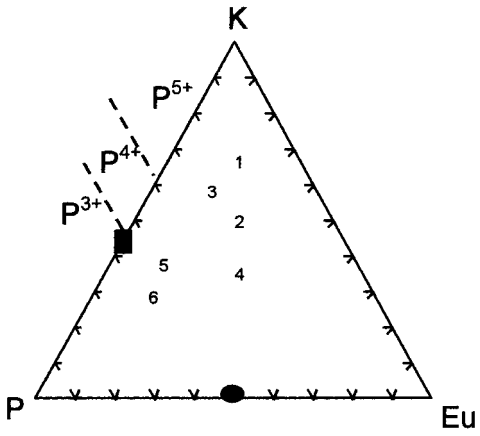

Figure 6. Eu−P−K phase diagram. Numbers represent the ratio of Eu−P−K in a particular reaction mixture. Shapes indicate the ratio of elements in a product formula disregarding Se: circle = $Eu_2P_2Se_6$, square = $K_6P_8Se_{18}$.

Table 13. Reactant Ratios Represented in Figure 6

phase diagram point	K/(K + P + Eu)	P/(K + P + Eu)	Eu/(K + P + Eu)	reaction product(s)
1	0.6667	0.1667	0.1667	
2	0.5	0.25	0.25	$K_4Eu(PSe_4)_2$
3	0.5714	0.2857	0.1429	
4	0.333	0.333	0.333	$KEuPSe_4$
5	0.375	0.5	0.125	$Eu_2P_2Se_6$
6	0.2857	0.5714	0.1429	$Eu_2P_2Se_6$ and $K_6P_8Se_{18}$

until at least a 45% phosphorus molar ratio, when $Eu_2P_2Se_6$ (points 5 and 6) was found. Another difference between the two phase diagrams is that we and others have not yet been able to synthesize a europium structure containing both P^V $(PSe_4)^{3-}$ and P^{IV} $(P_2Se_6)^{4-}$ units. It would be expected to be found in the region of the phase diagram between 40% and 50% phosphorus. Future experiments may reveal these selenophosphate units, but not within this Se^0/Se^{2-} phase space or under our reaction conditions. We do observe the $K_6P_8Se_{18}$ structure (point 6), indicating a region of the phase diagram above 55% phosphorus where selenophosphate units containing P^{III} can be found. As was the case in the lanthanum phase diagram, tie-lines can be drawn between different products on the basis of their element ratios. Point 6, for example, lies on a line that ties phase **V** to $K_6P_8Se_{18}$.

These phase diagrams can be used in conjunction with a formula developed by Kanatzidis to predict these types of structures.[31] We have modified the initial formula to include the four terms shown in eq 1.

$$(A_4P_2Se_6)_l(A_3PSe_4)_m(La_4(P_2Se_6)_3)_n(LaPSe_4)_o \qquad (1)$$

In this formula, $La_4(P_2Se_6)_3$ and $LaPSe_4$ are the parent structures for a RE^{3+} cation with $(P_2Se_6)^{4-}$ and $(PSe_4)^{3-}$ units, respectively. $A_4P_2Se_6$ and A_3PSe_4 comprise each base anionic unit with the appropriate number of alkali-metal cations to balance the charge. In the case where lanthanum is the RE cation, the structures of $KLaP_2Se_6$, $K_2La(P_2Se_6)_{1/2}(PSe_4)$, $K_3La(PSe_4)_2$, $K_4La_{0.67}(PSe_4)_2$, and $K_{9-x}La_{1+x/3}(PSe_4)_4$ ($x = 0$) can be derived from eq 1 as seen in Table 14. For example, one can think of breaking up the $La_4(P_2Se_6)_3$ parent structure by adding a $(P_2Se_6)^{4-}$ anionic unit with four alkali-metal cations to charge balance the new structure whose empirical formula is the phase $KLaP_2Se_6$.

Table 14. *l*−*o* Values, Predicted Formulas, and Reported Structures for $(A_4P_2Se_6)_l(A_3PSe_4)_m(La_4(P_2Se_6)_3)_n(LaPSe_4)_o$

l	m	n	o	predicted formula	reported structure
0	1	0	0	A_3PSe_4	K_3PSe_4[50]
1	0	0	0	$A_4P_2Se_6$	$K_4P_2Se_6$[50]
0	0	1	0	$La_4(P_2Se_6)_3$	
0	0	0	1	$LaPSe_4$	
1	0	1	0	$A_4La_4(P_2Se_6)_4$	$KLaP_2Se_6$[27]
1	0	0	2	$A_4La_2(P_2Se_6)(PSe_4)_2$	$K_2La(P_2Se_6)_{1/2}(PSe_4)$
0	1	0	1	$A_3La(PSe_4)_2$	$K_3La(PSe_4)_2$
0	2	0	1	$A_6La(PSe_4)_3$	$K_4La_{0.67}(PSe_4)_2$
0	3	0	1	$A_9La(PSe_4)_4$	$K_{9-x}La_{1+x/3}(PSe_4)_4$

Table 15. *l*−*o* Values, Predicted Formulas, and Reported Structures for $(A_4P_2Se_6)_l(A_3PSe_4)_m(Eu_2(P_2Se_6))_n[(Eu_3(PSe_4)_2]_o$

l	m	n	o	predicted formula	reported structure
0	0	1	0	$Eu_2P_2Se_6$	$Eu_2P_2Se_6$
0	0	0	1	$Eu_3(PSe_4)_2$	
1	0	1	0	$A_4Eu_2(P_2Se_6)_2 \equiv A_2EuP_2Se_6$	
0	1	0	1	$A_3Eu_3(PSe_4)_3$	$KEuPSe_4$
0	4	0	1	$A_{12}Eu_3(PSe_4)_6$	$K_4Eu(PSe_4)_2$[10]
0	7	0	1	$A_{21}Eu_3(PSe_4)_9 \equiv A_7Eu(PSe_4)_3$	
0	10	0	1	$A_{30}Eu_3(PSe_4)_{12} \equiv A_{10}Eu(PSe_4)_4$	

Table 15 contains formulas for compounds described by eq 2, which has been slightly modified from eq 1 to account for the divalent Eu(II) cation. In this formula, two parent structures have changed to $Eu_2(P_2Se_6)$ and $Eu_3(PSe_4)_2$.

$$(A_4P_2Se_6)_l(A_3PSe_4)_m(Eu_2(P_2Se_6))_n[(Eu_3(PSe_4)_2]_o \qquad (2)$$

These formulas, combined with the appropriate phase diagram, can be used to predict new structure compositions and the reaction conditions necessary to synthesize them. For example, eq 2 can be used to predict the formula $A_{10}Eu(PSe_4)_4$, which should be analogous to the homoleptic "$K_9La(PSe_4)_4$" cluster structure, and $K_7Eu(PSe_4)_3$, which should be analogous to **III**. However, these structures have eluded us to date.

The positions of phases **II**−**IV** in Figure 5 and their low dimensionality may help explain why $K_{9-x}La_{1+x/3}(PSe_4)_4$ ($x = 0.5$) was found instead of $K_9La(PSe_4)_4$. $KLaP_2Se_6$ and $K_2La(P_2Se_6)_{1/2}(PSe_4)$ are both two-dimensional layered structures. $K_3La(PSe_4)_2$ contains one-dimensional chains. $K_4La_{0.67}(PSe_4)_2$ also contains one-dimensional chains, but one could say that its dimensionality is actually lower than that of $K_3La(PSe_4)_2$ since the lanthanum position is only 2/3 occupied. The $K_{9-x}La_{1+x/3}(PSe_4)_4$ structure also contains these chains with a partially occupied lanthanum position, but the structure also contains isolated $[La(PSe_4)_4]$ clusters. In other words, one can imagine a relative continuum from an infinite chain structure to a relatively short chain structure when going from $K_3La(PSe_4)_2$ to $K_4La_{0.67}(PSe_4)_2$, followed by short chains and clusters in $K_{9-x}La_{1+x/3}(PSe_4)_4$, terminating at "$K_9La(PSe_4)_4$", which has no chain structure at all but only isolated $^0_\infty[La(PSe_4)_4]^{9-}$ anionic units as in $Rb_9Ce(PSe_4)_4$.[30] Within the phase diagram, the lines separating the $K_3La(PSe_4)_2$, $K_4La_{0.67}(PSe_4)_2$, and $K_{9-x}La_{1+x/3}(PSe_4)_4$ structures are not precisely defined. Therefore, the formation of $K_9La(PSe_4)_4$, with its isolated $^0_\infty[La(PSe_4)_4]^{9-}$ clusters, might not be as thermodynamically stable under our conditions as a structure with a few short chains in addition to isolated clusters as in the $K_{9-x}La_{1+x/3}(PSe_4)_4$ ($x = 0.5$) structure. Figure 7 compares the lanthanum coordination geometry looking down the $^1_\infty[La_{0.67}(PSe_4)_2]^{4-}$ chains in $K_4La_{0.67}(PSe_4)_2$ and a $^0_\infty[La(PSe_4)_4]^{9-}$ molecular anion in "$K_9La(PSe_4)_4$". The similarity of these coordination environ-

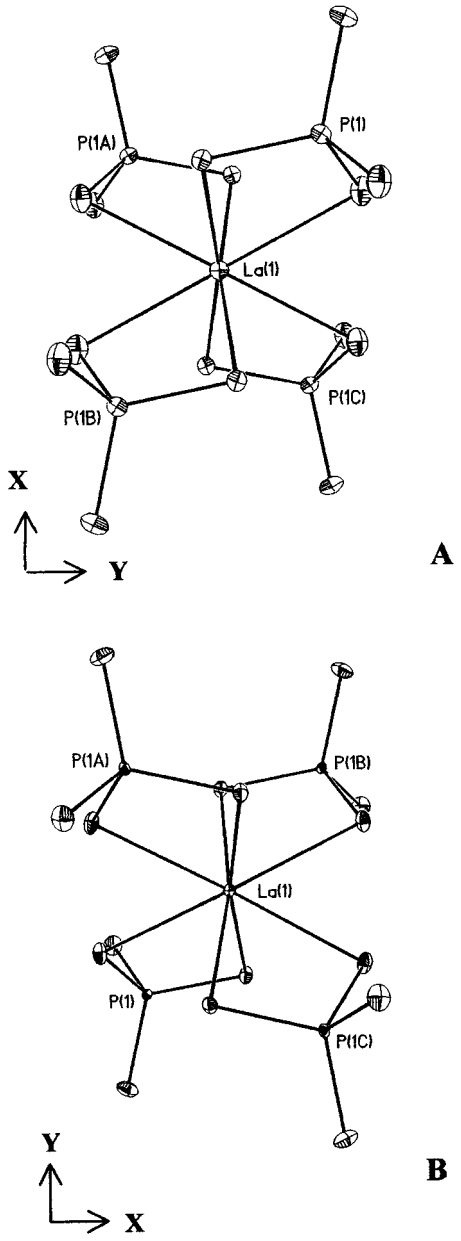

Figure 7. ORTEP plots of lanthanum coordination environments in $K_4La_{0.67}(PSe_4)_2$ and $K_{9-x}La_{1+x/3}(PSe_4)_4$. Thermal ellipsoids plotted at the 50% probability level. (A) View down $[La_{0.67}(PSe_4)_2]^{4-}$ chains. (B) $[La(PSe_4)_4]^{9-}$ isolated cluster.

ments shows how the difference in these compounds is only related to certain positions being occupied by lanthanum or potassium. This is supported by noting that the monoclinic unit cell of the expected stoichiometric $K_9La(PSe_4)_4$ can be related to a unit cell similar to $K_4La_{0.67}(PSe_4)_2$ by converting it [a = 21.1980(1) Å, b = 10.3100(1) Å, c = 18.2874(1) Å, β = 115.541(1)°] to an orthorhombic cell through a transposition of the b axis and c axis and halving the new b axis to obtain a = 19.126 Å, b = 9.1437 Å, and c = 10.3100 Å. In addition, the cell of $K_4La_{0.67}(PSe_4)_2$ can be transformed into the cell of $K_{9-x}La_{1+x/3}(PSe_4)_4$ ($x = 0.5$) by transposing and doubling the x and y axes.

Vibrational and Electronic Spectroscopy. Solid-state Raman spectroscopy has been performed on compounds **II**−**V**. The Raman spectra, shown in Figure 8, clearly show the four Raman-active vibrational modes of the tetrahedral $(PSe_4)^{3-}$ unit when compared to the $(PS_4)^{3-}$ tetrahedral unit in K_3PS_4.[49] Table

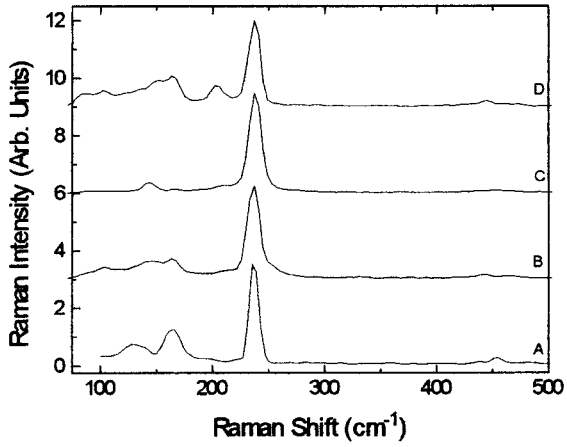

Figure 8. Solid-state Raman spectra: (A) $KEuPSe_4$, (B) $K_3La(PSe_4)_2$, (C) $K_4La_{0.67}(PSe_4)_2$, (D) $K_{9-x}La_{1+x/3}(PSe_4)_4$.

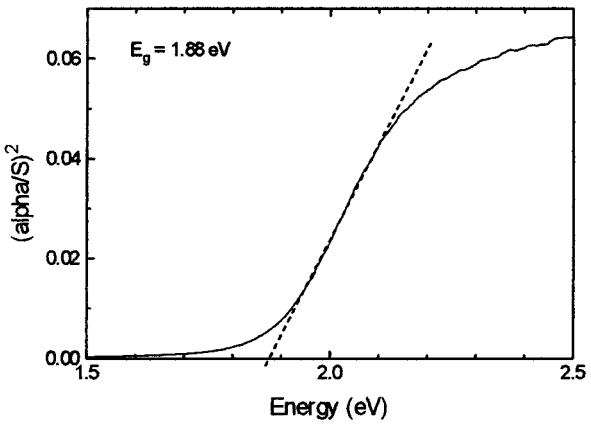

Figure 9. Optical band gap of $KEuPSe_4$.

Table 16. Raman Peaks (cm^{-1}) of Compounds **II**−**V**

	$(PS_4)^{3-}$ (T_d)[49]	$KEuPSe_4$	$K_3La(PSe_4)_2$	$K_4La_{0.67}(PSe_4)_2$	$K_{9-x}La_{1+x/3}(PSe_4)_4$
$\upsilon_3(F_2)$	548	454	443	454	446
$\upsilon_1(A_1)$	416	237	237	237	237, 200
$\upsilon_4(F_2)$	270	165	163	166	164
$\upsilon_2(E)$	215	130	145, 103	144	102

16 lists the peaks observed. The intense peak near 237 cm^{-1} is attributed to the totally symmetric stretch, and the small peak around 454 cm^{-1} is attributed to the asymmetric stretch. Bands below 200 cm^{-1} can be assigned to the bending vibrations of the $(PSe_4)^{3-}$ unit. The Raman spectrum of **IV** shows a peak at 200 cm^{-1} that is much larger than in the other three Raman spectra. The $(PSe_4)^{3-}$ tetrahedra in isolated $[La(PSe_4)_4]^{9-}$ clusters in $K_{9-x}La_{1+x/3}(PSe_4)_4$ would be expected to have much more freedom of motion, which may be represented by this intense peak.

Diffuse reflectance optical band gap measurements have been performed on $KEuPSe_4$. Figure 9 shows a plot of $(\alpha/s)^2$ vs energy. Extrapolation shows that $KEuPSe_4$ is likely a semiconductor with an optical band gap of 1.88 eV.

Conclusions

Compounds **I**−**V** have been synthesized by the reactive flux method and their structures determined by single-crystal X-ray diffraction. These compounds all contain $(PSe_4)^{3-}$ and/or

(49) Muller, A.; Mohan, N.; Cristophlienk, P.; Tossidis, I.; Drager, M. *Spectrochim. Acta* **1973**, *29A*, 1345.
(50) Briggs Piccoli, P. M.; Evenson, C. R.; Dorhout, P. K. Unpublished structures.

$(P_2Se_6)^{4-}$ anionic units. The presence of these two units in many other structures reported in the literature indicates they are quite thermodynamically stable. By using a Gibbs-type phase diagram analysis of these flux reactions, it was possible to understand what reaction conditions were necessary to form phases that comprise these units. K−P−RE phase diagrams have been constructed that indicate the molar ratios necessary to stabilize these units within phases in two K−P−RE−Se systems. Knowing what type of anionic unit will form under various conditions allows for a rational search for new materials. Current synthesis of yttrium analogues will show the effects of 4d transition metals on these structures.

Acknowledgment. This work was supported by the National Science Foundation (Grant CHE-9625378) and a NSF-MRI Instrumentation Grant. We thank Dr. Victor Young, University of Minnesota, for helpful crystallographic discussions.

Supporting Information Available: Tables of additional crystallographic details, all bond distances and angles, anisotropic thermal parameters, and ORTEP views of **I** and **V**. This material is available free of charge via the Internet at http://pubs.acs.org.

IC000595Z